Optics Letters

# Surface nanoscale axial photonics at a capillary fiber

T. Hamidfar,[1,2] A. Dmitriev,[2] B. Magdan,[3] P. Bianucci,[1] and M. Sumetsky[2,*]

[1]Concordia University, Montreal, Québec H4B 1R6, Canada
[2]Aston Institute of Photonic Technologies, Aston University, Birmingham B4 7ET, UK
[3]OFS Laboratories, 19 Schoolhouse Road, Somerset, New Jersey 08873, USA
*Corresponding author: m.sumetsky@aston.ac.uk

Received 10 May 2017; revised 11 June 2017; accepted 14 June 2017; posted 16 June 2017 (Doc. ID 295540); published 3 August 2017

**We present the theory and first experimental demonstration, to the best of our knowledge, of a sensing platform based on surface nanoscale axial photonics (SNAP) at a capillary fiber. The platform explores optical whispering gallery modes, which circulate inside the wall of a capillary and slowly propagate along its axis. Due to the small thickness of the capillary wall, these modes are sensitive to spatial and temporal variations of the refractive index of the media adjacent to the internal capillary surface. In particular, the developed theory allows us to determine the internal effective radius variation of the capillary from the measured mode spectra. Experimentally, a SNAP resonator is created by local annealing of the capillary with a focused $CO_2$ laser followed by internal etching with hydrofluoric acid. The comparison of the spectra of this resonator in the cases when it is empty and filled with water allows us to determine the internal surface nonuniformity introduced by etching. The results obtained pave the way for a novel advanced approach in sensing of media adjacent to the internal capillary surface and, in particular, in microfluidic sensing.**



***OCIS codes:*** (060.2340) Fiber optics components; (060.2370) Fiber optics sensors; (140.3945) Microcavities; (230.3990) Micro-optical devices; (280.4788) Optical sensing and sensors.

https://doi.org/10.1364/OL.42.003060

The sensing platform developed in this Letter extends the surface nanoscale axial photonics (SNAP) platform [1–3] to the case of thin-walled capillary fibers, including those filled with gas, liquid, or solid media. Following the idea of Ref. [4], we explore whispering gallery modes (WGMs), which circulate inside the capillary wall and slowly propagate along the capillary axis for sensing the media adjacent to the internal capillary surface and, in particular, the nonuniformity of the internal surface itself. The wavelength of WGMs considered is very close to their cutoff wavelength. For this reason, the propagation constant of these modes is small and their speed along the capillary axis is slow [3]. It has been shown that the axial distribution of slow WGMs is sensitive to extremely small nanoscale variations of the optical fiber radius [1]. In the case of a capillary fiber, it is of great interest to investigate how the spatial and temporal variations of the media adjacent to the internal capillary surface affect the spectrum of the SNAP resonator created at the capillary wall. In particular, it is important to find out if it is possible to determine the *internal effective radius variation* of the capillary from the measured spectra, as was done for the outer radius in SNAP [1–3].

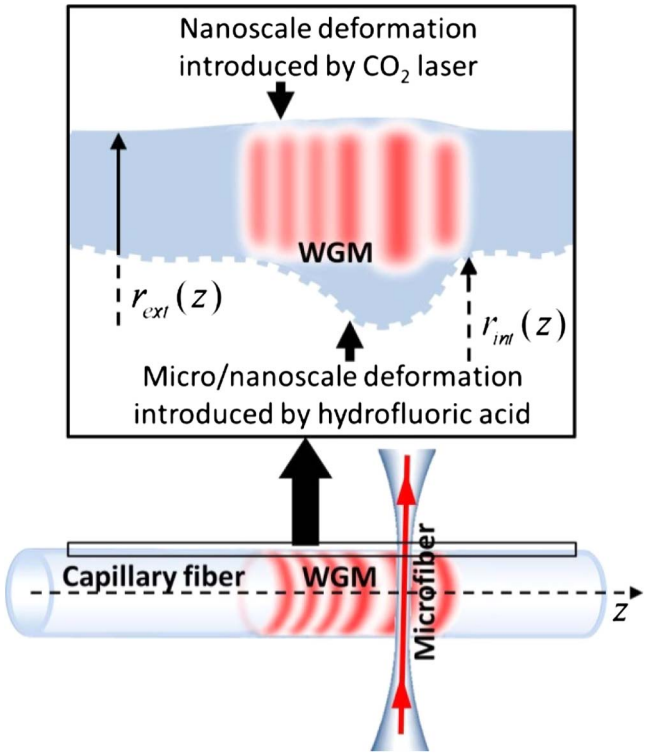


**Fig. 1.** Illustration of a capillary fiber coupled to an input–output microfiber. The capillary was processed with a $CO_2$ laser beam and, internally, with hydrofluoric acid. Inset: magnified cross section of the capillary wall (not to scale).

Our method illustrated in Fig. 1 bridges and extends the ideas of the liquid core resonance sensing method [5] and SNAP [1]. White, Oveys, and Fan [5] proposed and demonstrated a fused silica capillary with a few-micron-thick wall acting as a WGM resonator sensor of the refractive index of liquid carried by the capillary. In their first demonstration and followup publications (see reviews [6,7]), an axially uniform silica capillary coupled to a transverse microfiber or planar waveguide was explored. Sensing of fluid inside the capillary was performed *locally at the position of the transverse waveguide* and was based on the measurement of variation of a single resonance. A SNAP microresonator introduced along the capillary surface (Fig. 1) can significantly advance this approach. In fact, it enables the detection of changes, which happen *away from the waveguide position* along the length of the resonator by controlling the variation of resonant spectra of this resonator [4].

The WGMs of our concern are adjacent to the external capillary surface. For a capillary with a thick wall, these modes have negligible overlap with the internal surface and, therefore, are independent of the optical properties of media situated at or in a small vicinity of this surface. For example, in the illustration of Fig. 1, the WGM is much less sensitive to the internal surface variations near the internal bump. Away from the bump, the wall becomes thinner and the WGMs spectra start reacting to the changes at the internal surface of the capillary.

In application to the capillary fibers, the SNAP theory is developed as follows. The dependence of external and internal radii of the capillary, $r_{\text{int}}(z) = r_{\text{int}}^{(0)} + \Delta r_{\text{int}}(z)$ and $r_{\text{ext}}(z) = r_{\text{ext}}^{(0)} + \Delta r_{\text{ext}}(z)$, are assumed to be adiabatically slow and the refractive index is defined as

$$n(\rho, z) = \begin{cases} n_{\text{int}}, & 0 < \rho \le r_{\text{int}}(z), \\ n_{\text{cap}}, & r_{\text{int}}(z) < \rho \le r_{\text{ext}}(z), \\ n_{\text{ext}}, & r_{\text{ext}}(z) < \rho. \end{cases} \tag{1}$$

The WGMs considered are numerated by the azimuthal quantum number $m$, radial quantum number $p$, and axial quantum number $q$ (the latter is introduced if the WGM is localized along the capillary axis) and can be expressed in the cylindrical coordinates as $E_{mpq}(z, \rho, \varphi) = \exp(im\varphi) Q_{mp}(\rho, z) \Psi_{mpq}(z)$. The slowness of WGMs is manifested in the small value of their propagation constant, $\beta(z)$, or, equivalently, in the proximity of their wavelength $\lambda$ to the cutoff wavelength $\lambda_{mp}^{(\text{cut})}(z)$ [8]. Functions $Q_{mp}(\rho, z)$ and $\Psi_{mpq}(z)$ are determined by the adiabatic separation of variables in the wave equation, which leads to the well-known equation for the radial distribution of modes in an optical fiber [9]:

$$\frac{d^2 Q_{mp}}{d\rho^2} + \frac{1}{\rho}\frac{dQ_{mp}}{d\rho} + \left( \left( \frac{2\pi n(\rho, z)}{\lambda} \right)^2 - \frac{m^2}{\rho^2} - \beta^2(z) \right) Q_{mp} = 0, \tag{2}$$

where the dependencies on the axial coordinate $z$ are parametric. Consequently, the dependence of $\Psi_{mpq}(z)$ on $z$ is determined by the one-dimensional wave equation

$$\frac{d^2 \Psi_{mpq}}{dz^2} + \beta^2(z) \Psi_{mpq} = 0. \tag{3}$$

Here we are interested in the situation when the variation of the cutoff wavelength, $\lambda_{mp}^{(\text{cut})}(z) - \lambda_{mp}^{(0)}$, and the deviation of the radiation wavelength from the cutoff, $\lambda - \lambda_{mp}^{(\text{cut})}(z)$, are small. This condition is satisfied for small variations of radii, $\Delta r_{\text{int}}(z)$ and $\Delta r_{\text{ext}}(z)$, and for the evanescent values of $Q_{mp}(\rho, z)$ near the internal wall surface. Under these assumptions, we set the propagation constant equal to

$$\beta(z) = \frac{2\pi n_{\text{cap}}}{\lambda_{mp}^{(\text{cut})}} \sqrt{\frac{2(\lambda - \lambda_{mp}^{(\text{cut})}(z))}{\lambda_{mp}^{(\text{cut})}}} \tag{4}$$

and ignore the terms that are of higher order in $\lambda - \lambda_{mp}^{(\text{cut})}(z)$. Then Eq. (2) is simplified to the following equation independent of wavelength $\lambda$:

$$\frac{d^2 Q_{mp}}{d\rho^2} + \frac{1}{\rho}\frac{dQ_{mp}}{d\rho} + \left( \left( \frac{2\pi n(\rho, z)}{\lambda_{mp}^{(\text{cut})}} \right)^2 - \frac{m^2}{\rho^2} \right) Q_{mp} = 0. \tag{5}$$

We are looking for the solution of this equation in the form

$$Q_{mp}(\rho, z) = \begin{cases} A J_m(k_{mp} n_{\text{int}} \rho), & 0 < \rho \le r_{\text{int}}(z), \\ B J_m(k_{mp} n_{\text{cap}} \rho) + C Y_m(k_{mp} n_{\text{cap}} \rho), & r_{\text{int}}(z) < \rho \le r_{\text{ext}}(z), \\ D J_m(k_{mp} n_{\text{ext}} \rho), & r_{\text{ext}}(z) < \rho. \end{cases} \tag{6}$$

Here $k_{mp} = 2\pi/\lambda_{mp}^{(\text{cut})}$, functions $J_m(x)$ and $Y_m(x)$ are the Bessel functions, and parameters $A$, $B$, $C$, and $D$ are determined from the condition of continuity of $Q_{mp}(\rho, z)$ and its derivative over $\rho$ at the interfaces $r_1(z)$ and $r_2(z)$ [10]. The solution of Eq. (6) with the refractive index profile determined by Eq. (1) allows us to express the cutoff wavelength, $\lambda_{mp}^{(\text{cut})}(z)$, through the external and internal radii, $r_{\text{ext}}(z)$ and $r_{\text{int}}(z)$. Next, to determine the WGMs and their spectrum, we solve Eq. (3) with the propagation constant determined by Eq. (4).

The device fabricated and investigated in this Letter consists of a silica fiber capillary with an external radius $r_0 = 21$ μm and an initial wall thickness of 6 μm. WGMs are excited in the capillary by a biconical fiber taper having a microfiber waist, which was fabricated of a conventional single-mode fiber. To measure the resonant spectrum of WGMs, the taper is connected to the optical spectrum analyzer.

A SNAP microresonator was introduced at the capillary surface by local annealing with a focused $CO_2$ laser beam. The WGM spectra of this resonator were measured at microfiber positions spaced by 20 μm along the capillary axis [Fig. 2(a)]. The length of the resonator was ~300 μm. From Fig. 2(a), the spectral width of the resonator is $\Delta\lambda_0 \sim 0.15$ nm at a radiation wavelength of $\lambda_0 \sim 1.57$ μm. The height of the introduced external effective radius variation (ERV) is estimated as $\Delta r_0 \sim \Delta\lambda_0 r_0/\lambda_0 \sim 2$ nm. The resonant spectra shown in Fig. 2(a) correspond to the vicinity of a cutoff wavelength having the azimuthal and radial quantum numbers $m \sim 2\pi n_{\text{cap}} r_0/\lambda_0$ and $p = 0$, respectively. For a silica capillary with $n_{\text{cap}} \sim 1.5$, we have $m \sim 100$.

In order to make the WGM spectrum of the SNAP microresonator sensitive to the presence of fluid inside the capillary, its wall thickness was reduced by internal etching with the hydrofluoric acid [5]. The etching process was controlled by the simultaneous measurement of the resonant spectrum and was stopped when the shift of resonances was observed.

Figures 2(b) and 2(c) show the SNAP resonator spectra after etching for the empty and the water-filled capillary, respectively. It is seen that the axial WGM resonances adjacent to the cutoff wavelength with the fundamental radial number series ($p = 0$, $q = 0, 1, 2, \ldots$, bottom) experience relatively small distortion. However, the axial resonances of WGMs with a lager radial quantum number (hypothetically the $p = 1$ series, top) change

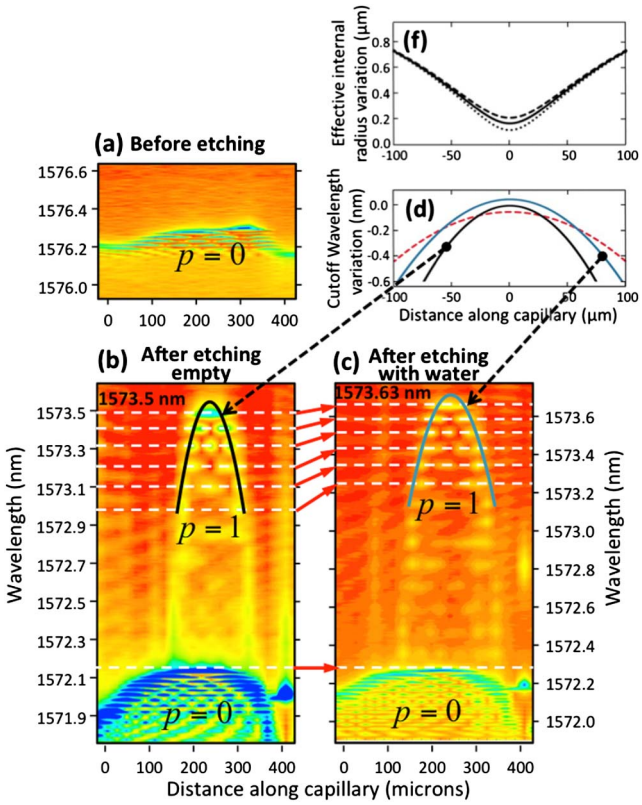


**Fig. 2.** Surface plots of spectra of the fabricated SNAP resonator measured with 20 μm resolution along the capillary axis. (a) Before etching, $p = 0$. (b) After etching, empty capillary, $p = 0$ (bottom) and $p = 1$ (top). (c) After etching, capillary filled with water, $p = 0$ (bottom) and $p = 1$ (top). (d) Parabolic approximation of the cutoff wavelength for the empty (black curve) and water-filled (blue curve) capillary. Dashed red curve is the difference of these curves. (f) The restored internal ERV. The solid, dashed, and dotted curves correspond to $\lambda_w - \lambda_e$ equal to 0.05 nm, 0.04 nm, and 0.06 nm, respectively.

dramatically. The $p = 0$ axial resonances are narrower, i.e., less lossy than the $p = 1$ resonances, due to the fact that they have less overlap with the internal surface of the capillary. The dramatic shrinking of the $p = 1$ WGMs compared to the $p = 0$ WGMs along the axial direction can be explained by the axial nonuniformity introduced by hydrofluoric etching. We suspect that, in addition to the nanoscale variation of the wall thickness, the $CO_2$ laser annealing deforms the capillary wall as a whole. This deformation disturbs the hydrofluoric acid flow and leads to the creation of a bump of the capillary wall illustrated in the inset of Fig. 1. While the $p = 0$ WGM series have small overlap with the internal wall surface and, therefore, are not noticeably sensitive to the appearance of this bump, it causes the additional localization of the $p = 1$ WGMs evident from Figs. 1(b) and 1(c).

Comparison of Figs. 2(b) and 2(c) shows that filling the capillary with water led to the reduction of separation between the axial series of resonances with axial quantum numbers $q = 0, 1, 2, \ldots$ clearly seen for the $p = 1$ series. In our experiment, adding water introduced the shift of the SNAP microresonator spectrum by 0.13 nm as a whole. This shift is presumably due to mechanical deformation of the capillary pressurized by water. Below, in the theoretical analysis of experimental data, we assumed that, besides this global shift, the effect of water on the $p = 0, q = 0$ resonances is negligible. This fact allowed us to calibrate the relative positions of surface plots in Figs. 2(b) and 2(c) by equalizing the positions of the $p = 0$, $q = 0$ resonances.

We used the developed theory to estimate the internal ERV, $r_{\text{int}}(z) = r_{\text{int}}^{(0)} + \Delta r_{\text{int}}(z)$, from the measured spectra of the SNAP resonator. To this end, we numerically analyzed and compared the $p = 1$ resonances for the empty and water-filled capillaries shown in Figs. 2(b) and 2(c), respectively. The major contribution to the appearance of these resonances was caused by variation of the internal radius $r_{\text{int}}(z)$. Therefore, in our calculations, we neglected the variation of the external radius. Figure 3(a) compares the dependencies of the cutoff wavelength on the internal radius for $r_{\text{int}}(z) \equiv r_0 = 21.12\,\mu\text{m}$, $n_{\text{cap}} = 1.46$, two azimuthal quantum numbers, $m = 113$ and 105, and three radial quantum numbers, $p = 0, 1, 2$. We suggest that our experimental situation can be approximated by the behavior of the $m = 113$, $p = 0$ and $m = 105$, $p = 1$ series. Figure 3(b) compares the deviations of dependencies shown in Fig. 3(a) from their value $\lambda_{mpq}^{(0)}$ for a thick capillary ($r_{\text{int}} < 16\,\mu\text{m}$) magnified to the nanometer wavelength scale of our interest. The curves in Fig. 3(b) look remarkably similar and coincide with good accuracy after the horizontal translation into the darker rectangle in this figure. Thus, all of them can be defined by a common function $\Delta\lambda^{(\text{cut})}(r_{\text{int}} + s)$ with the appropriate choice of shift $s$. Consequently, the internal ERV can be found as $\lambda_{mpq}^{(\text{cut})}(r_{\text{int}}) = \Delta\lambda^{(\text{cut})}(r_{\text{int}} + s) + \lambda_{mpq}^{(0)}$. While the actual value of $s$ is not important for the determination of *variation* of the internal radius, the direct application of this result to our experiment is complicated because the accurate measurement of $\lambda_{mpq}^{(0)}$ is not possible. To solve this problem, we proceed as follows. Figures 3(c) and 3(d) compare the behavior of cutoff wavelength with $m = 113$ and $q = 0, 1, 2$ for the

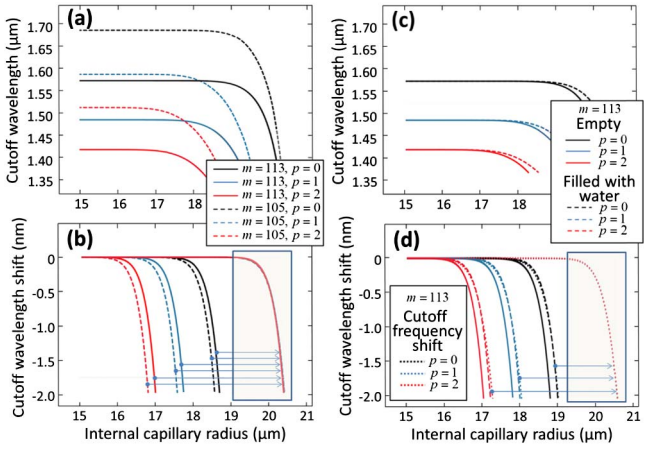


**Fig. 3.** (a) Cutoff wavelength as a function of internal ERV for the quantum numbers indicated on the plot. (b) Dependencies shown in (a) magnified and shifted along the vertical axis. (c) Cutoff wavelength as a function of internal ERV for the empty and water-filled capillaries for the quantum numbers indicated on the plot. (d) Dependencies shown in (c) magnified and shifted along the vertical axis. Curves shown in (b) and (d) are compared by horizontal translation into the darker rectangles.

empty capillary and the capillary filled with water. These dependencies, again, coincide with a good accuracy after horizontal translation [they are compared in the darken rectangles of Figs. 3(c) and 3(d)]. In particular, the shift of the cutoff wavelength caused by filling the capillary with water is defined by a common function:

$$\widetilde{\Delta\lambda}^{(\mathrm{cut})}(r_{\mathrm{int}}+s)=\lambda_{mpq}^{(\mathrm{cut})}(r_{\mathrm{int}}+s)|_{\mathrm{water}}-\lambda_{mpq}^{(\mathrm{cut})}(r_{\mathrm{int}}+s)|_{\mathrm{empty}}, \tag{7}$$

which does not depend on $\lambda_{mpq}^{(0)}$. Thus, this function does not depend on the actual values of the azimuthal and radial quantum numbers $m$ and $p$, respectively, which were not precisely determined from the experiment.

In both cases of empty and water-filled capillaries, we estimate the cutoff wavelength dependency corresponding to $p=1$ spectral series in Figs. 2(b) and 2(c) by parabolas, $\lambda_{\mathrm{water}}^{(\mathrm{cut})}(z)=\lambda_w-\gamma_w z^2$ and $\lambda_{\mathrm{empty}}^{(\mathrm{cut})}(z)=\lambda_e-\gamma_e z^2$, respectively. Here parameters $\gamma_{w,e}$ are expressed through the separation of resonances along the axial quantum number, $\delta\lambda_{w,e}$, as $\gamma_{w,e}=2(\pi n_{\mathrm{cap}}\delta\lambda_{w,e})^2\lambda_0^{-3}$ [11]. From Figs. 2(b) and 2(c), setting the top of the $p=0$ resonance series as a reference (which, as noted above, has a negligible effect of water), we estimate $\delta\lambda_e\sim 0.1$ nm, $\delta\lambda_w\sim 0.08$ nm, and $\lambda_w-\lambda_e\sim 0.05$ nm. Consequently, $\gamma_w=-1.1\cdot 10^{-7}$ μm$^{-1}$ and $\gamma_e=-6.9\cdot 10^{-8}$ μm$^{-1}$. Figure 2(d) shows the dependencies $\lambda_{\mathrm{empty}}^{(\mathrm{cut})}(z)$ and $\lambda_{\mathrm{water}}^{(\mathrm{cut})}(z)$ (black and blue curves, respectively), which are translated into surface plots on Figs. 2(b) and 2(c) and show good agreement with the experiment. Finally, the black solid curve in Fig. 2(f) shows the internal ERV $\Delta r_{\mathrm{int}}(z)$ restored from the difference $\lambda_{\mathrm{water}}^{(\mathrm{cut})}(z)-\lambda_{\mathrm{empty}}^{(\mathrm{cut})}(z)$ [red dashed curve in Fig. 2(d)] following Eq. (7). This variation appears to be quite different from parabola and has the micrometer scale. In contrast, as it follows from the SNAP theory of a regular fiber [1–3], the same cutoff wavelength variation can be introduced by the external ERV $\Delta r_{\mathrm{ext}}(z)=(\lambda_{\mathrm{empty}}^{(\mathrm{cut})}(z)-\lambda_{mpq}^{(0)})\,r_0/\lambda_0$, which has nanometer rather than micrometer scale.

In summary, we have developed a theory of a capillary SNAP platform and experimentally demonstrated a SNAP microresonator at the surface of a capillary that is sensitive to the presence of fluid inside the capillary. The resonator was created by local annealing of the capillary with a focused $CO_2$ laser beam and internal etching with hydrofluoric acid. We investigated the variation of the spectra of fabricated microresonator resulted from thinning of the capillary wall and the presence of water inside the capillary. Using the developed theory, we determined the internal effective radius variation of the capillary from the spectra of the SNAP resonator measured experimentally. We believe that the future development of this theory will allow for the simultaneous determination of the internal and external effective radius variation of the capillary. In addition, we suggest that the developed approach will allow for the determination of the complex structure of microfluidic components adjacent to the internal capillary surface, e.g., the resonant structure of microparticles [12]. Generally, this demonstration provides the groundwork for advanced microfluidic sensing with SNAP microresonators.

**Funding.** Royal Society (WM130110); Horizon 2020 Framework Programme (H2020) (H2020-EU.1.3.3, 691011); Engineering and Physical Sciences Research Council (EPSRC) (EP/P006183/1).

**Acknowledgment.** MS acknowledges the Royal Society Wolfson Research Merit Award.

## REFERENCES AND NOTES

1. M. Sumetsky, D. J. DiGiovanni, Y. Dulashko, J. M. Fini, X. Liu, E. M. Monberg, and T. F. Taunay, Opt. Lett. **36**, 4824 (2011).
2. M. Sumetsky, Nanophotonics **2**, 393 (2013).
3. M. Sumetsky, Phys. Rev. Lett. **111**, 163901 (2013).
4. M. Sumetsky, Opt. Lett. **39**, 5578 (2014).
5. I. M. White, H. Oveys, and X. Fan, Opt. Lett. **31**, 1319 (2006).
6. X. Fan and I. M. White, Nat. Photonics **5**, 591 (2011).
7. T. Reynolds, N. Riesen, A. Meldrum, X. Fan, J. M. M. Hall, T. M. Monro, and A. Francois, Laser Photon. Rev. **11**, 1600265 (2017).
8. The fact that the cutoff wavelengths of the WGMs with very large azimuthal quantum numbers $m$ correspond to the zero propagation constant, $\beta=0$, does not contradict to the well-known relation $k_{mp}n_{\mathrm{ext}}<\beta<k_{mp}n_{\mathrm{cap}}$ for small $m$ (see, e.g., [9]).
9. A. W. Snyder and J. Love, *Optical Waveguide Theory* (Chapman and Hall, 1983).
10. For the case $k_{mp}n_{\mathrm{cap}}r_0\approx m\gg 1$ and $k_{mp}n_{\mathrm{ext}}r_0<m$ considered, the Bessel function $J_m(k_{mp}n_{\mathrm{ext}}\rho)$ exponentially decays with the growth of $\rho$ for $0<k_{mp}n_{\mathrm{ext}}(\rho-r_0)\ll m$.
11. M. Sumetsky and J. M. Fini, Opt. Express **19**, 26470 (2011).
12. Y. Li, F. Abolmaali, K. W. Allen, N. I. Limberopoulos, A. Urbas, Y. Rakovich, A. V. Maslov, and V. N. Astratov, Laser Photon. Rev. **11**, 1600278 (2017).